Effects of physical parameters on the cell-to-dendrite transition in directional solidification*

Wei Lei(魏 雷), Lin Xin(林 鑫)†, Wang Meng(王 猛), and Huang Wei-Dong(黄卫东)

State Key Laboratory of Solidification Processing, Northwestern Polytechnical University, Xi'an 710072, *China*

(Received 31 October 2014; revised manuscript received 27 January 2015; published online 29 May 2015)

A quantitative cellular automaton model is used to study the cell-to-dendrite transition (CDT) in directional solidification. We give a detailed description of the CDT by carefully examining the influence of the physical parameters, including: the Gibbs–Thomson coefficient Γ, the solute diffusivity D_l, the solute partition coefficient k_0, and the liquidus slope m_l. It is found that most of the parameters agree with the Kurz and Fisher (KF) criterion, except for k_0. The intrinsic relations among the critical velocity V_{cd}, the cellular primary spacing $\lambda_{c,max}$, and the critical spacing λ_{cd} are investigated.

Keywords: directional solidification, cell-to-dendrite transition, dendrite growth, cellular automaton

PACS: 81.30.–t, 68.70.+w, 81.30.Fb, 81.10.Aj **DOI:** 10.1088/1674-1056/24/7/078108

1. Introduction

The solidification microstructure determines the properties of the final product. The directional solidification of binary alloys can produce planar, cellular, and dendritic interfaces.[1–12] The transition from planar to cellular interface can be well established by the Mullins–Sekerka instability theory.[1] When the growth velocity V exceeds a threshold value V_c, the planar interface transients into a steady state cellular microstructure of wavelength λ_c. The depth of the cellular groove can be short, that is: shallow cell. A cellular groove can also be long, that is: deep cell. For even higher velocities, deep cells change into dendrites. The cell-to-dendrite transition (CDT) has been investigated for decades. However, the criterion of transition from a cellular to a dendritic microstructure has not been well established. Kurz and Fisher[2] have proposed that $V_{cd} = V_c/k_0$ (V_{cd} = growth velocity of cellular–dendrite transition, V_c = planar growth stability limit, and k_0 = solute partition coefficient). Trivedi[3] presented a minimum in the solute Peclet number p, which supported Kurz and Fisher (KF) criterion. Laxmanan *et al.*[4] concluded that the KF criterion was doubtful, except for succinonitrile-acetone (SCN-ace) and Al–2% Cu alloys. Other alloys, such as SCN–Salol and Pb–Sn, did not support the KF criterion.

The onset of the sidewise instability has recently been investigated through the examination of the local spacing λ_{cd} of the CDT by Georgelin and Pocheau,[8] and Trivedi *et al.*[9,10] They found that cells and dendrites coexist over a range of velocities under fixed temperature gradient G and initial composition C_0. Within the transition zone, a critical spacing λ_{cd} is found, under which dendrites transform into cells and above which cells transform to dendrites. Georgelin and Pocheau[8] analyzed an expression of the critical side-branching spacing, that is $V\lambda_{cd}^2 G^{1/4} =$ constant. Teng *et al.*[10] presented a different expression: $\lambda_{cd} = A(D_l\Gamma)^{1/3}(G/V)^{-1/3}C_0^{-1/4}$, where A is a constant, D_l is the diffusion coefficient, and Γ is the Gibbs–Thomson coefficient. They also concluded that the CDT initiates when the maximum cell spacing $\lambda_{c,max}$ equals λ_{cd}. At the end of the CDT, the minimum dendrite spacing $\lambda_{d,min} = \lambda_{cd}$. According to $\lambda_{c,max} = \lambda_{cd}$, one can obtain the general expression for the lower limit of the CDT. Gurevich *et al.*[23] have shown that there is a major difference between two- and three-dimensional configurations in the PF simulations. Furthermore, it was shown that the CDT is extremely sensitive to anisotropy.[23,31] Echebarria *et al.* [24] have found that the CDT cannot be understood by the phase field model without taking into account the thermodynamic noise.

To obtain a deep understanding of the CDT, the accuracy of the expressions of $\lambda_{c,max}$, $\lambda_{d,min}$, and λ_{cd} should be quantitatively examined to void incorrect formulas. The relationship among λ_{cd}, G, V, and C_0 has been quantitatively established by thin-film experiments. However, in experiments, the physical parameters, such as the Gibbs–Thomson coefficient Γ, the solute diffusivity D_l, the solute partition coefficient k_0, and the liquidus slope m_l, cannot be exhaustively surveyed. To quantitatively examine the influence of physical parameters on the CDT, numerical simulation is the only option. The phase-field model[13–26] has a nontrivial computational challenge to survey this problem. In this paper, a quantitative cellular automaton (CA) model[32–35] is used to investigate the influence of physical parameters on the CDT in directional solidification.

*Project supported by the National Natural Science Foundation of China (Grant Nos. 51271213 and 51323008), the National Basic Research Program of China (Grant No. 2011CB610402), the National High Technology Research and Development Program of China (Grant No. 2013AA031103), the Specialized Research Fund for the Doctoral Program of Higher Education of China (Grant No. 20116102110016), and the China Postdoctoral Science Foundation (Grant No. 2013M540771).

†Corresponding author. E-mail: xlin@nwpu.edu.cn

© 2015 Chinese Physical Society and IOP Publishing Ltd

In this paper, various CDT morphologies are simulated with different strengths of physical parameters while keeping the other parameters unchanged.

2. Numerical model

The computational domain is divided into a Cartesian grid. Each grid, which is also called a cell, is characterized by the following three states: liquid, solid, and interface, as seen in Fig. 1. To govern the transition of cell states, a capture rule is needed to control the evolution of different states. A solid fraction (i.e. solid cell $f_s = 1$, liquid cell $f_s = 0$, and interface cell $0 < f_s < 1$) is introduced to implicitly capture the solid–liquid interface. The growth of solid fractions can be calculated according to the interface kinetics, which is also based on the algorithms of the interface curvature calculation and the thermal or mass transport calculation. The thermal and mass transport calculation methods can be found elsewhere.[28–30] The following subsections focus on the capture rule, interface curvature calculation, and the interface growth kinetics.

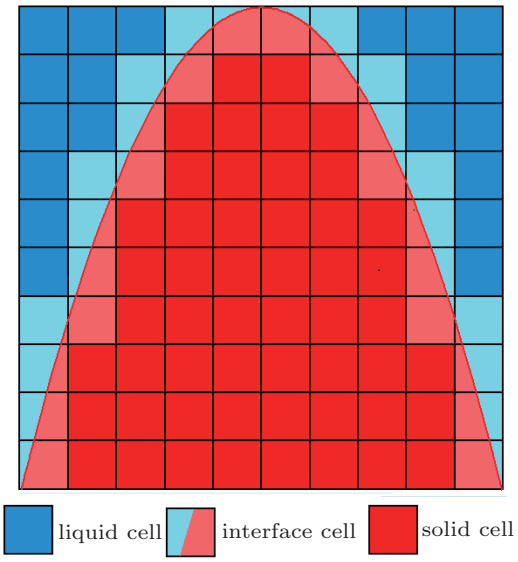


Fig. 1. (color online) The scheme of solid–liquid interface in CA model: liquid cell, interface cell, and solid cell.

2.1. Capture rule

During the CA simulation, the transition of the cell state from liquid to interface is governed by the capture rule. Since the transition of cell states influences the growth of solid–liquid interface, the capture rule used in the CA model should be carefully selected. The traditional capture rules, such as von Neumann's and Moore's rules, were evidenced to have strong artificial anisotropy.[28] The capture rule in the present CA model used a limited neighbor solid fraction (LNSF) method,[35] which is the modification of the von Neumann's rule.

Based on the von Neumann's rule, the LNSF method calculates the averaged solid fraction $f_{s_{ave}}$ around a specific liquid cell. If $f_{s_{ave}}$ is larger than a constant value $f_{s_{const}}$, then the liquid cell can be captured by von Neumann's rule. Otherwise, if $f_{s_{ave}}$ is less than $f_{s_{const}}$, then the liquid cell cannot be captured, even if it is satisfied by von Neumann's rule. The LNSF method was effective for the pure substance CA mode,[35] in which the artificial anisotropy could be reduced to a large extent. More importantly, the LNSF method is only based on some basic algebraic operators, which means that the LNSF method is as computationally efficient as von Neumann's rule. In the present work, the LNSF method was applied to the simulation of directional solidification.

2.2. Interface curvature calculation

The accuracy in curvature calculation has a significant influence on the accuracy of the CA model. As far as is known, the most popular method for the simulation of interface curvature is the counting cell method.[28]

However, the counting cells method is not accurate enough for quantitative simulation.[28] A more accurate method is based on the variation of the unit vector normal (VUVN) to the solid–liquid interface along the direction of the interface,[29]

$$K = \frac{2\frac{\partial f_s}{\partial x}\frac{\partial f_s}{\partial y}\frac{\partial^2 f_s}{\partial x \partial y} - \left(\frac{\partial f_s}{\partial y}\right)^2 \frac{\partial^2 f_s}{\partial x^2} - \left(\frac{\partial f_s}{\partial x}\right)^2 \frac{\partial^2 f_s}{\partial y^2}}{\left[\left(\frac{\partial f_s}{\partial x}\right)^2 + \left(\frac{\partial f_s}{\partial y}\right)^2\right]^{3/2}}. \quad (1)$$

The VUVN method needs to calculate the derivatives of solid fraction, which are difficult to be precisely calculated in a sharp interface model. A bilinear interpolation method was used in the CA model, the detail of which can be found in Ref. [32].

2.3. Interface growth kinetics

The interface growth kinetics used in this paper are proposed by Zhu and Stefanescu as[29]

$$C_l^* = C_0 + \frac{T_l^{eq} - T^* - \Gamma K f(\varphi, \theta_0)}{m_l}, \quad (2)$$

$$\Delta f_s = (C_l^* - C_l^{old})/[C_l^*(1 - k_0)], \quad (3)$$

$$C_l^{new} = C_l^{old}/[1 - (1 - k_0)\Delta f_s], \quad (4)$$

where C_l^{new} and C_l^{old} are the actual concentrations at different time steps.

3. Results and discussion

The alloys for the simulations of the CDT are succinonitrile–0.1 mol% acetone (SCN–0.1 mol% ace) and SCN–0.2 wt% Salol, the thermal physical parameters are shown in Table 1.

Table 1. Thermal physical parameters of succinonitrile (SCN), SCN-acetone, and SCN-Salol.

	Parameters	Values
Succinonitrile	latent heat (L)	3.705×10^{3} J·mol^{-1}
	melting point ($T_{\rm m}$)	331.233 K
	heat capacity ($C_{\rm p}$)	160.15 J·mol^{-1}·K^{-1}
	thermal diffusivity (α)	1.134×10^{-7}m^2·s^{-1}
	Gibbs–Thomson coefficient (Γ)	6.62×10^{-8} m·K
Succinonitrile-acetone	diffusion coefficient in the liquid ($D_{\rm l}$)	1.27×10^{-9} m^2·s^{-1}
	liquidus slope ($m_{\rm l}$)	–2.16 K·mol^{-1}·pct^{-1}
	equilibrium partition coefficient (k_0)	0.103
Succinonitrile-Salol	diffusion coefficient in the liquid ($D_{\rm l}$)	0.8×10^{-9} m^2·s^{-1}
	liquidus slope ($m_{\rm l}$)	–0.68 K·wt^{-1}·pct^{-1}
	equilibrium partition coefficient (k_0)	0.16

The computational domain is 256 μm×2048 μm for the 2D model, and the mesh size is 1.0 μm. If the simulation needs more resolution, then the computational domain of 512 μm×4096 μm can be used. At the beginning of the simulations, the bottom of the computational domain is a planar interface.

According to the KF criterion, $V_{\rm cd} = V_{\rm c}/k_0 = D_{\rm l}G/(\Delta T_0 k_0) = D_{\rm l}G/[m_{\rm l}C_0(k_0-1)]$, and Γ has no effects on the CDT.

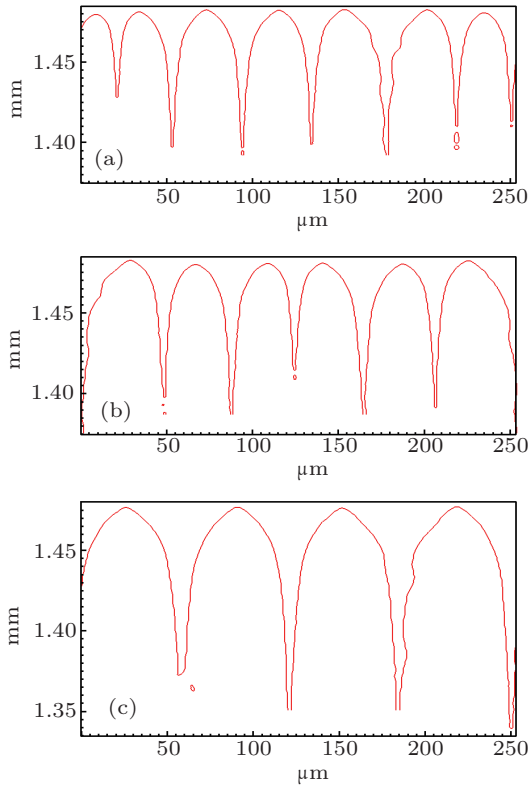


Fig. 2. (color online) The simulated morphologies of SCN-ace alloy with different strengths of Gibbs–Thomson coefficient Γ. (a) $\Gamma = 3.2\times10^{-8}$ m·K, $G = 15$ K/mm, $V = 100$ μm/s, (b) $\Gamma = 6.4\times10^{-8}$ m·K, $G = 15$ K/mm, $V = 100$ μm/s, (c) $\Gamma = 9.6\times10^{-8}$ m·K, $G = 15$ K/mm, $V = 100$ μm/s.

Figure 2 shows the simulation results with different Γ under unchanged conditions of $V = 100$ μm/s, $G = 15$ K/mm, $C_0 = 0.1$ mol%, $m_{\rm l} = -2.16$ K/mol%, $k_0 = 0.103$, and $\varepsilon = 0.005$. When Γ increases from 3.2×10^{-8} m·K to 9.6×10^{-8} m·K, both the cell and the dendrite spacings increase. However, it can be obviously seen that the changing of Γ has no effects on the CDT. The influence of Γ on the CDT agrees well with the KF criterion.

By using the same strategy, the solute diffusivity $D_{\rm l}$, the initial composition C_0, and the liquidus slope $m_{\rm l}$ are also examined by the CA simulations, as shown in Figs. 3–5. The corresponding changes in pulling velocities V or temperature gradient G are calculated according to the KF criterion. The simulation results show that the three physical parameters: $m_{\rm l}$, C_0, and $D_{\rm l}$ also agree well with the prediction of the KF criterion.

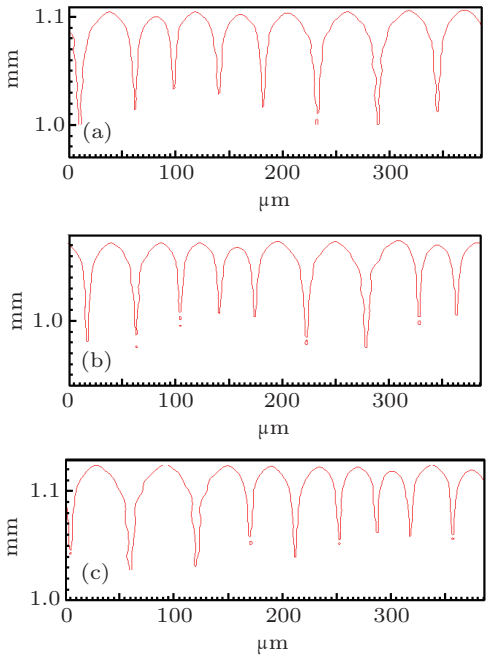


Fig. 3. (color online) The simulated morphologies of SCN-ace alloy with different strengths of the solute diffusivity $D_{\rm l}$, while keeping $D_{\rm l}/V$ constant. (a) $D_{\rm l} = 0.635\times10^{-9}$ m^2/s, $G = 15$ K/mm, $V = 50$ μm/s, (b) $D_{\rm l} = 1.27\times10^{-9}$ m^2/s, $G = 15$ K/mm, $V = 100$ μm/s, (c) $D_{\rm l} = 1.91\times10^{-9}$ m^2/s, $G = 15$ K/mm, $V = 150$ μm/s.

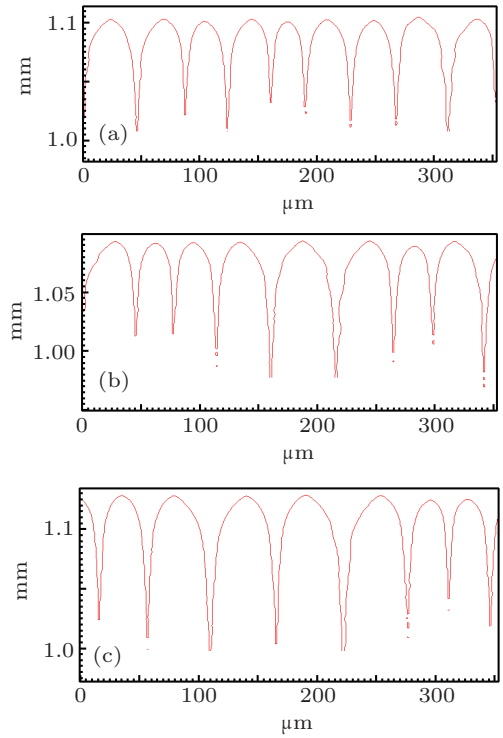


Fig. 4. (color online) The simulated morphologies of SCN-ace alloy with different strengths of the initial composition C_0, while keeping G/C_0 constant. (a) $C_0 = 0.20$, $G = 30$ K/mm, $V = 100$ μm/s, (b) $C_0 = 0.1$, $G = 15$ K/mm, $V = 100$ μm/s, (c) $C_0 = 0.0667$, $G = 10$ K/mm, $V = 100$ μm/s.

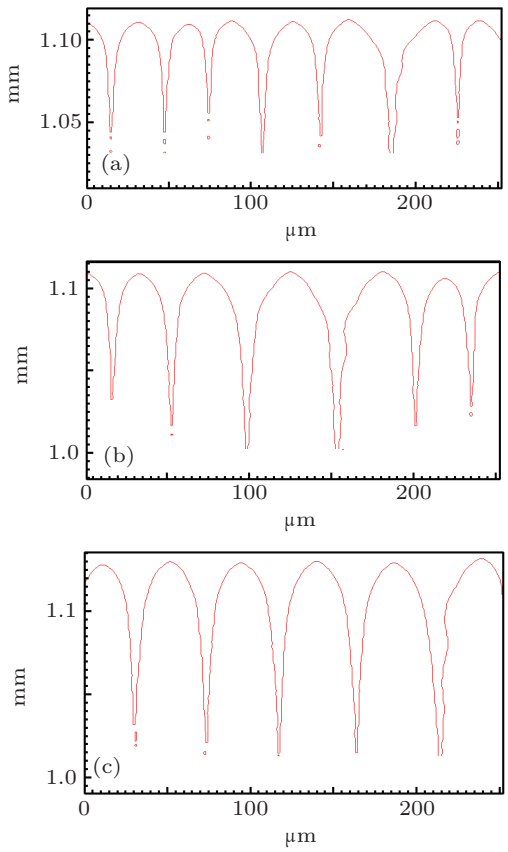


Fig. 5. (color online) The simulated morphologies of SCN-ace alloy with different strengths of the liquidus slope m_l, while keeping $m_l V$ constant. (a) $m_l = -1.44$, $G = 15$ K/mm, $V = 150$ μm/s, (b) $m_l = -2.16$, $G = 15$ K/mm, $V = 100$ μm/s, (c) $m_l = -2.88$, $G = 15$ K/mm, $V = 75$ μm/s.

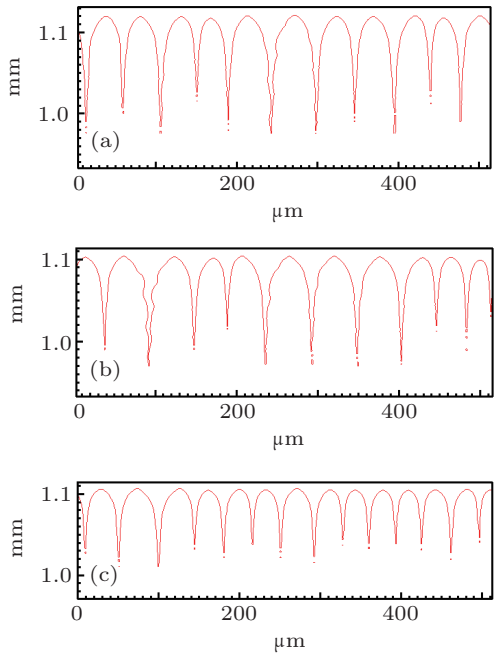


Fig. 6. (color online) The simulated morphologies of SCN-ace alloy with different strengths of the solute partition coefficient k_0, while keeping $(1-k_0)V$ constant. (a) $k_0 = 0.04$, $G = 15$ K/mm, $V = 93.87$ μm/s, (b) $k_0 = 0.10$, $G = 15$ K/mm, $V = 100.00$ μm/s, (c) $k_0 = 0.16$, $G = 15$ K/mm, $V = 106.99$ μm/s.

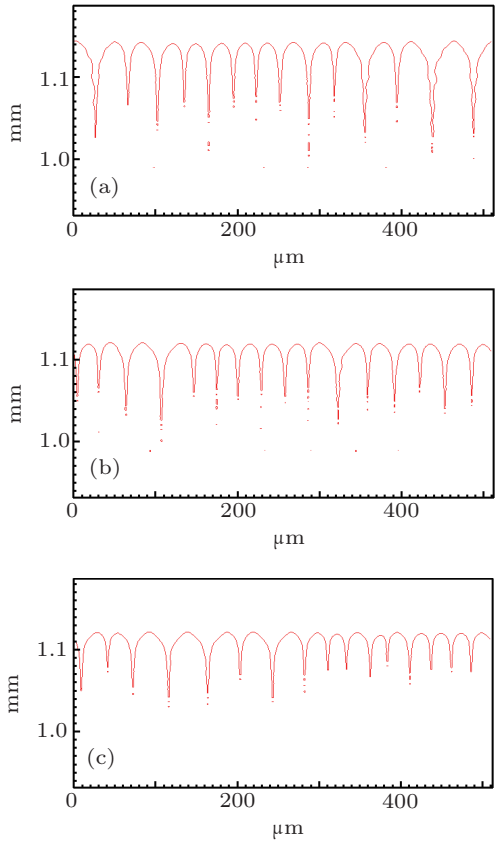


Fig. 7. (color online) The simulated morphologies of SCN-Salol alloy with different strengths of the solute partition coefficient k_0, while keeping $(1-k_0)V$ constant. (a) $k_0 = 0.04$, $G = 15$ K/mm, $V = 93.91$ μm/s, (b) $k_0 = 0.10$, $G = 15$ K/mm, $V = 100.00$ μm/s, (c) $k_0 = 0.16$, $G = 15$ K/mm, $V = 107.04$ μm/s.

However, the solute partition coefficient k_0 is very exceptional, which is the main finding of this paper. During the

simulations, k_0 was continually increased from 0.04 to 0.16 by an interval of 0.01. The pulling velocities were set close to the prediction of the KF criterion. Figures 6 (SCN-0.1 mol% ace) and 7 (SCN-0.2 wt% Salol) show the influence of k_0 on the CDT, in which only $k_0 = 0.04$, 0.10, and 0.16 are presented. The simulation results show that when k_0 is small, the simulated morphologies are the CDT; and, when k_0 is large, the morphologies are cellular. Figure 8 is the 3D simulation of the SCN-0.1 mol% ace with different k_0. By comparing the 2D and 3D simulation results, it can be concluded that a similar influence pattern of k_0 on the CDT is obtained. Overall, both the 2D and the 3D CA simulations show that the KF criterion is only validated when k_0 is small.

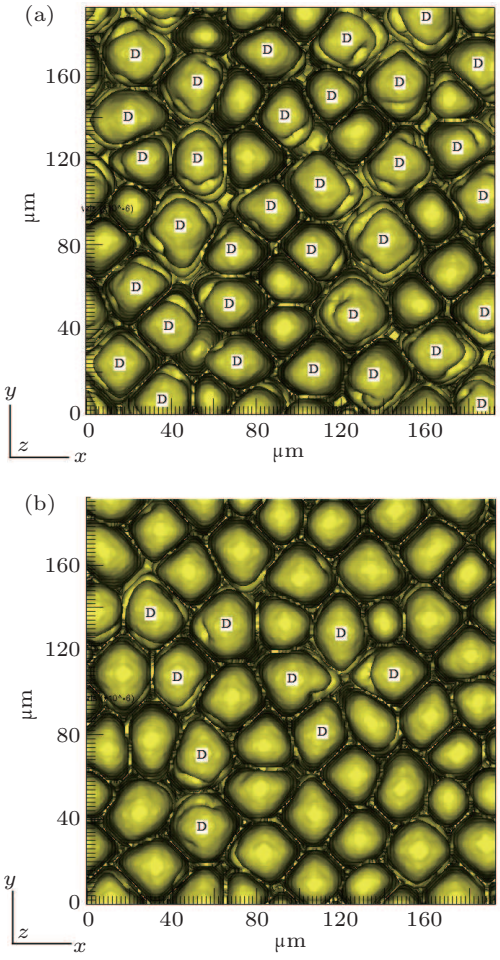


Fig. 8. (color online) The 3D simulations of the CDT for SCN-ace alloy with solute partition coefficient conditions: (a) $k_0 = 0.10$, $G = 15$ K/mm, $V = 100$ μm/s, (b) $k_0 = 0.20$, $G = 15$ K/mm, $V = 112.5$ μm/s.

To quantitatively understand the CDT, the relationship between $\lambda_{c,max}$ and λ_{cd} should be analyzed. Teng *et al.*[10] have presented an expression of the λ_{cd} by investigating through a thin film experiment

$$\lambda_{cd} = 80.79\left(\frac{1-k_0}{k_0}C_0\right)^{-1/4}\left(\frac{\varepsilon_4 D\Gamma}{GV}\right)^{1/3}, \tag{5}$$

and Georgelin and Pocheau have presented a different expression of the λ_{cd}

$$\lambda_{cd} = 445.384(D\Gamma)^{3/4}V^{-1/2}G^{-1/8}C_0^{-1/2}. \tag{6}$$

Hunt and Lu[27] presented a rough expression for the cell spacings. The phase field simulations[13,23] evidenced that the relationship between the maximum finger spacing and the pulling velocity is $\lambda_{c,max}^2 V$ = constant. Based on the phase field simulations, the Hunt–Lu expression is modified into

$$\lambda_{c,max} = B_1 k_0^{-1/3}\left(\frac{\Gamma}{m_l C_0(k_0-1)}\right)^{1/2}\left(\frac{D_l}{V}\right)^{1/2}, \tag{7}$$

where B_1 is constant.

Based on the investigations in present CA simulations and the KF criterion, the critical velocity V_{cd} of the CDT should follow the expression

$$V_{cd} = B_2 f(\varepsilon)g(k_0)\frac{GD_l}{m_l C_0}, \tag{8}$$

where B_2 is constant, $f(\varepsilon)$ and $g(k_0)$ are the unknown expressions of ε and k_0.

By solving $\lambda_{cd} = \lambda_{c,max}$, one can obtain the expression of V_{cd}. Since equations (6) and (7) have the same $V^{-1/2}$, the V_{cd} cannot be obtained based on the two formulas. Equation (5) is selected to be a more appropriate formula to describe the λ_{cd}. To get consistent results with Eq. (8), equations (5) and (7) are modified slightly as

$$\lambda_{cd}^{\text{modified}} = B_3\left(\frac{1-k_0}{k_0}m_l C_0\right)^{-1/3}\left(\frac{\varepsilon_4 D_l\Gamma}{GV}\right)^{1/3}, \tag{9}$$

$$\lambda_{c,max}^{\text{modified}} = B_4 k_0^{-1/3}G^{-1/6}\Gamma^{1/3}\left(\frac{1}{m_l C_0(k_0-1)}\right)^{1/2} \times\left(\frac{D_l}{V}\right)^{1/2}, \tag{10}$$

where B_3 and B_4 are constant.

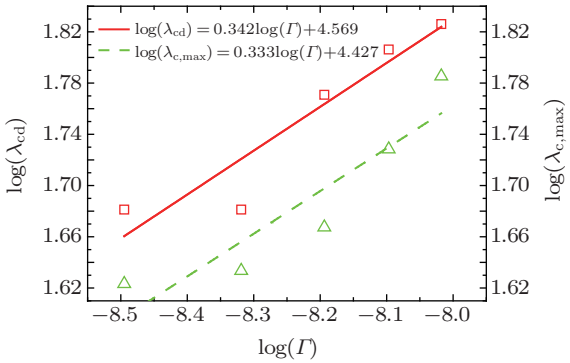


Fig. 9. (color online) Plots of $\log(\lambda_{cd})$–$\log(\Gamma)$ and $\log(\lambda_{c,max})$–$\log(\Gamma)$ based on the data in the present CA simulations.

The modifications are based on the following considerations. The $\lambda_{cd} \propto C_0^{-1/4}$ in Eq. (5) is modified into $\lambda_{cd} \propto C_0^{-1/3}$ in this paper to obtain a consistent result. In Trivedi's experiment,[10] it is found that $\lambda_{cd} \propto C_0^{-0.27}$, which is also close to $\lambda_{cd} \propto C_0^{-1/3}$, since it is difficult to accurately measure

C_0 in the experiments. Using the data in Fig. 2, the relationship between λ_{cd} and Γ is established to $\lambda_{cd} \propto \Gamma^{1/3}$, as shown in Fig. 9. The relationship of $\lambda_{c,max} \propto \Gamma^{1/3}$ can also be obtained in Fig. 9. Hence, the expression of Γ should be modified into $\Gamma^{1/3}$, as seen in Eq. (7). In Eq. (7), the temperature gradient $G^{-1/6}$ is a guess that is made to have a consistent formula.

Overall, based on Eqs. (8)–(10), one can get a self-consistent relationship among $\lambda_{c,max}$, $\lambda_{cd,}$ and V_{cd}. By solving $\lambda_{cd} = \lambda_{c,max}$, we can obtain the exact expression of V_{cd}. However, the influence of the interface energy anisotropy ε on the $\lambda_{c,max}$ and λ_{cd} are still unknown. Therefore, the influences of k_0 and ε should be quantitatively investigated later.

4. Conclusions

In conclusion, the influences of the physical parameters (Γ, D_l, m_l,C_0) on the cell-to-dendrite transition in directional solidification are investigated by using CA simulations. It is evidenced that Gibbs–Thomson coefficient Γ has no effects on the CDT. It is also found that the influences of the physical parameters (D_l, m_l,C_0) exactly follow the Kurz and Fisher (KF) criterion. The most important finding in this paper is that when k_0 is small, the influences of k_0 on the CDT agree with the KF criterion; and, when k_0 is larger than 0.16, the V_{cd} is higher than the prediction of the KF criterion. The special performance of k_0 on the CDT could explain why SCN-ace and SCN-Salol have different behaviors on the CDT. Based on the simulation results, the expressions of the cell spacing $\lambda_{c,max}$ and the critical spacing λ_{cd} are modified to give a consistent formula to predict the CDT.

References

[1] Mullins W W and Sekerka R F 1964 *J. Appl. Phys.* **35** 444
[2] Kurz W and Fisher D J 1981 *Acta Metal.* **29** 11
[3] Trivedi R 1984 *Metall. Trans. A* **15** 977
[4] Tewari S N and Laxmanan V 1987 *Metall. Trans. A* **18** 167
[5] Karma A and Pelce P 1989 *Europhys. Phys. Lett.* **9** 713
[6] Trivedi R and Kurz W 1994 *Inter. Mater. Rev.* **39** 49
[7] Liu L X and Kirkaldy J S 1995 *Acta Metall. Mater.* **43** 2891
[8] Georgelin M and Pocheau A 1998 *Phys Rev. E* **57** 3189
[9] Trivedi R, Shen Y and Liu S 2003 *Metall. Mater. Trans. A* **34** 395
[10] Teng J, Liu S and Trivedi R 2009 *Acta Mater.* **57** 3497
[11] Huang W D, Geng X D and Zhou Y H 1993 *J. Cryst. Growth* **134** 105
[12] Lin X, Huang W D, Feng J, Li T and Zhou Y H 1999 *Acta Mater.* **47** 3271
[13] Lan C W, Shih C J and Lee M H 2005 *Acta Mater.* **53** 2285
[14] Takakia T, Fukuokaa T and Tomita Y 2005 *J. Crys. Growth* **283** 263
[15] Warren J A and Boettinger W J 1995 *Acta Metall. Mater.* **43** 689
[16] Greenwood M, Haataja M and Provatas N 2004 *Phys. Rev. Lett.* **93** 246101
[17] Karma A and Rappel W J 1998 *Phys. Rev. E* **57** 4323
[18] Karma A 2001 *Phys. Rev. Lett.* **87** 115701
[19] Kim S G, Kim W T and Suzuki T 1999 *Phys. Rev. E* **60** 7186
[20] Plapp M and Dejmek M 2004 *Europhys. Phys. Lett.* **65** 276
[21] Provatas N, Greenwood M, Athreya B, Goldenfeld N and Dantzig J 2005 *Inter. J. Mod. Phys. B* **19** 4525
[22] Provatas N, Wang Q Y, Haataja M and Grant M 2003 *Phys. Rev. Lett.* **91** 155502
[23] Gurevich S, Karma A, Plapp M and Trivedi R 2010 *Phys. Rev. E* **81** 011603
[24] Echebarria B, Karma A and Gurevich S 2010 *Phys. Rev. E* **81** 021608
[25] Xing H, Wang J Y, Chen C L, Jin K X and Du L F 2014 *Chin. Phys. B* **23** 038104
[26] Wang Z J, Wang J C and Yang G C 2010 *Chin. Phys. B* **19** 078101
[27] Hunt J D and Lu S Z 1996 *Metal. Mater. Trans. A* **27** 611
[28] Sanchez L B and Stefanescu D M 2004 *Metall. Mater. Trans. A* **35** 2471
[29] Zhu M F and Stefanescu D M 2007 *Acta Mater.* **55** 1741
[30] Dong H B and Lee P D 2005 *Acta Mater.* **53** 659
[31] Chen M W, Chen Y C, Zhang W L, Liu X M and Wang Z D 2014 *Acta Phys. Sin.* **63** 038101 (in Chinese)
[32] Wei L, Lin X, Wang M and Huang W D 2012 *Acta Phys. Sin.* **61** 098104 (in Chinese)
[33] Wei L, Lin X, Wang M and Huang W D 2011 *Appl. Phys. A* **103** 123
[34] Wei L, Lin X, Wang M and Huang W D 2012 *Com. Mater. Sci.* **54** 66
[35] Wei L, Lin X, Wang M and Huang W D 2012 *Physica B* **407** 2471